ELSEVIER

Materials Science and Engineering A231 (1997) 170–182

MATERIALS SCIENCE & ENGINEERING A

Fatigue crack growth resistance in SiC particulate and whisker reinforced P/M 2124 aluminum matrix composites

J.J. Mason [a,*], R.O. Ritchie [b]

[a] *University of Notre Dame, Department of Aerospace and Mechanical Engineering, 365 Fitzpatrick Hall, Notre Dame, IN, 46556-5637, USA*
[b] *Materials Sciences Division, Lawrence Berkeley National Laboratory and Department of Materials Science and Mineral Engineering, University of California, Berkeley, CA, 94720-1760, USA*

Received 13 January 1997; revised 10 March 1997

Abstract

Fatigue crack growth is examined in P/M 2124 aluminum alloys reinforced with SiC particles (SiC_p) and whiskers (SiC_w) over a wide spectrum of growth rates from 10^{-12} to 10^{-4} m per cycle. Effects of aging treatment, orientation of crack growth direction with respect to the rolling direction, mean stress (or stress ratio), and reinforcement volume percent on the fatigue crack growth threshold are investigated in terms of crack tip shielding mechanisms. Comparison to fatigue crack growth in the unreinforced alloy indicates that crack growth resistance in the composites is superior to the monolithic alloy at low stress intensity ranges, ΔK. Specifically, at the lower growth rates the superior crack growth resistance of the composites is due to the formation of tortuous crack paths and a consequently enhanced roughness induce crack closure. Fatigue response near threshold is found to be relatively insensitive to changes in aging treatment with observed variations reflecting the associated changes in plastic behavior. In whisker reinforced composites, the orientation of the crack with respect to the rolling direction had a significant effect on fatigue crack growth rate while in the particulate reinforced composites orientational effects were not significant. Increasing the volume fraction resulted in higher crack growth resistance at low growth rates in the particulate reinforced materials. At high stress ratios, resistance in both whisker and particulate reinforced composites was lowered, and the measured fatigue crack propagation threshold, ΔK_{th}, was found to be independent of the reinforcement morphology and volume percent. © 1997 Elsevier Science S.A.

Keywords: Fatigue crack growth; Aluminium alloys; Shielding mechanisms

1. Introduction

Metal matrix composites (MMCs) exhibit a combination of properties not found in monolithic metals. The addition of high modulus fibers, particles, nodules or whiskers (or combinations thereof) to conventional alloys can result in favorable changes in strength, elastic modulus, wear resistance, creep resistance, coefficient of thermal expansion and fatigue life. In addition, although second phase additions can result in a loss of tensile ductility, lower fracture toughness, and an increase in density, specific properties of the composite are usually improved enough to provide considerable weight savings potential in load bearing and high temperature applications. In particular, they offer widespread potential due to their essentially isotropic properties and substantially improved strengths and stiffnesses compared to unreinforced alloys. There are many systems of MMCs available; however, due to the economical production of silicon carbide whiskers (SiC_w) and particles (SiC_p) [1] and the ease of fabrication of SiC_p and SiC_w, reinforced aluminum composites with standard metallurgical and mechanical processing, considerable interest has been directed toward aluminum alloys discontinuously reinforced with SiC.

Load bearing applications will often require components to endure cyclic stress, and, consequently, good fatigue characterization of these materials is required. Systematic studies of a fundamental nature relating mechanistically the role of composite microstructure in controlling fatigue resistance in these materials have indicated that many factors may be important in determining the fatigue resistance of SiC/Al composite materials including: processing, matrix properties, reinforcement properties, matrix/reinforcement inter-

* Corresponding author. Tel: +219 631 9370; E-mail: mason.12@nd.edu

PII S09 1-5093(97)00086-5

Table 1
Nominal chemical composition limits (weight percent): wrought aluminum 2124

Copper	Magnesium	Manganese	Iron	Zinc	Silicon	Titanium	Chromium
3.8–4.9	1.2–1.8	0.30–0.9	0.30	0.25	0.20	0.15	0.10

face properties, and reinforcement volume percent, morphology, size and distribution within the matrix [2–21]. Accordingly this investigation is focused on determining which factors serve a primary role in the mechanisms of fatigue crack resistance in the studied aluminum matrix composites discontinuously reinforced with SiC.

Published studies on aluminum matrix composite systems discontinuously reinforced with SiC [2–21] have demonstrated the dependence of fatigue resistance and fatigue crack growth rate upon some of these factors. Shang and Ritchie [9] report the dependence of fatigue crack propagation stress intensity threshold range, ΔK_{th}, upon the particulate size and volume percent for an Al-Zn-Mg-Cu alloy (similar to Al 7091) reinforced with 15 and 20 vol.% SiC_p. Coarser particles, nominally 16 μm in diameter, resulted in stress intensity threshold measurements of approximately 4.0 MPa-$m^{1/2}$ at $R = 0.1$ while smaller reinforcement, nominally 5 μm in diameter, produced lower threshold values of approximately 3.0 MPa-$m^{1/2}$. This behavior was explained in terms of roughness induced closure mechanisms and crack tip trapping by the SiC particles. The composites examined by Shang and Ritchie also exhibited significant crack tip bridging by unbroken ligaments. [11] The formation of these ligaments was attributed to the early fracture of SiC_p ahead of the crack tip. This type of behavior had a significant effect at higher growth rates (high ΔK), but at lower growth rates it was negligible. The lower volume percent material resulted in lower threshold stress intensity ranges due to lower closure loads. Botstein et al. [19] measured crack growth rates in the mid-growth rate (Paris Law) regime for Al 2014-40% SiC_p and Al 7091-30% SiC_p materials. They determined a threshold stress intensity range of approximately 7.0 MPa-$m^{1/2}$ for Al 2014-40% and indicated that particle clustering enhances crack growth so that crack growth rates in this material are much higher than in Al 7091-30% SiC_p. A 3.7 Cu–1.4 Mg aluminum alloy with 20% $SiCu_w$ studied by Lee [20] exhibited dramatically deflected crack growth. Indeed, the crack deflection prohibited the gathering of any data, but fractography showed evidence of whisker pull-out on the crack faces indicating this as a possible mechanism for crack tip bridging in this material. Ratnaparkhi and Rack [21] reported similar results although they found that crack deflection did not occur at lower crack driving forces; any fatigue crack propagation rates were not reported. Knowles and King [8] report that crack growth rates in the Paris law regime increase with increased levels of aging while fatigue crack growth thresholds were quite similar for 20% SiC_p/Al 8090 in different aging conditions with 3 μm particles. In a parallel work these same authors [5] indicate that the particle/matrix interface has effects only at high ΔK for the same composite system. For a 15% SiC_p/Al 2014 material, Davidson [6] reports that crack surface roughness has little effect on closure in a 15% SiC_p/Al 2014 composite. Sugimura and Suresh [4] report the same trend and attribute it to the fracture of particles ahead of the crack tip. Several authors [2,7] have reported a strong influence of residual stress on the fatigue behavior. Prestraining of the specimen is reported to have positive effects. A high temperature soak of 20% SiC_p/Al 2124 materials is also reported to have dramatically positive effects on fatigue response due to the dissolution of coarse intermetallics.

In the present study, fatigue crack propagation behavior in a 2124 aluminum alloy reinforced with either silicon carbide whiskers (SiC_w) or particles (SiC_p) is examined with special emphasis on the role of aging condition, volume percent, crack growth orientation and load ratio on the fatigue crack growth threshold condition. Of particular interest is developing the ability to measure crack growth rates in the whisker materials and identifying the active crack tip shielding mechanisms at low crack growth rates.

2. Experimental procedures

The aluminum matrix composites examined in this study involved three volume fractions of reinforcement, namely 15, 20 and 30 vol.%, and two different reinforcement morphologies, whisker and particulate, all with the same powder metallurgy (P/M) processed 2124 aluminum alloy matrix. The composition of the P/M Al 2124 alloy is listed in Table 1. Two particulate reinforced materials were studied, 20 vol.%, 70 and 30 vol.% SiC_p/Al 2124, and one whisker material was studied, 15 vol.% SiC_w/Al 2124. The composites were received in 'as extruded' plate form. The particulate composites were manufactured by DWA Specialties, Inc., while the whisker composite was manufactured by ARCO Metals, Silag Operations. Both companies use similar proprietary P/M techniques. results will be compared with P/M unreinforced and wrought alloys.

Table 2
Tensile data for SiC/Al 2124

Vol. %	Rolling direction	Young's modulus (GPa)	Aging condition	Yield strength (MPa)	U.T.S. (MPa)	Elongation[a] %	K_{Ic} (MPa$\sqrt{m}$)
0	L-T		OA	370	440	10.2	—
		72.5	PA	447	479	10.0	—
			UA[b]	360	488	17.8	—
15 SiC_w	L-T	94.3	OA	465	589	2.9	15.1
			PA	504	690	3.0	15.3
			UA[b]	501	650	3.5	19.3
	T-L	83.3	OA	403	487	4.8	13.2
			UA	432	568	6.4	18.4
20 SiC_p	L-T	108	OA	403	561	4.0	11.3
			PA	509	567	2.9	14.0
			UA	445	580	4.1	11.8
30 SiC_p	L-T	127	OA	487	541	1.9	15.9
			PA	609	660	1.7	17.6
			UA	526	618	1.9	18.9
	T-L	125	OA	496	542	2.1	17.9
			UA	447	557	2.3	17.6

[a] On 25 mm gauge length.
[b] T351 (other UA are T851).

The extruded plates were solution heat treated at 477°C for 1 h and water quenched to room temperature. Concern over the existence of residual thermal stresses in the material due to the large difference in thermal expansion between the matrix and carbide motivated the inclusion of a 2% compression along the short-transverse direction before aging. After compression, the composites were artificially aged at 177°C for various times and water quenched to room temperature. Three aging conditions, under-aged, peak-aged and over-aged, were identified corresponding to aging times of 1, 5 and 50 h, respectively. Due to the accelerated aging kinetics of the composites, [22,23] these times are shorter than the typical aging times used to achieve similar aging conditions in the unreinforced alloy. It was found that the aging kinetics were independent of reinforcement morphology and volume percent.

The mechanical properties of all alloys/microstructures tested are shown in Table 2. Characteristic increases in the strength and modulus of the composite over the unreinforced alloy are apparent, with corresponding decreases in toughness and ductility. Uniaxial tensile failure usually occurred in a brittle fashion with failure initiating at a surface flaw. Plane strain fracture toughness was measured as per ASTM E-399 [24] on compact tension, C(T), specimens identical to those used in the fatigue studies.

Characterization of the reinforcement volume percent, size, morphology and distribution within the matrix revealed that the whiskers were about 1 μm in diameter with an average aspect ratio (length over diameter) of 4. Rolling of the whisker reinforced material during processing resulted in the alignment of the whiskers along the rolling direction. The degree of alignment was not complete, however, as seen in Fig. 1(a). Indeed, low magnification micrographs reveal bands of high reinforcement concentration along the rolling direction. (Fig. 1(b)). The 20 vol.% particulate reinforced material is shown in Fig. 2. The particulate reinforcement was generally larger than the whisker reinforcement with at average equivalent-area diameter of 10 μm and an average aspect ratio of 1.75. Very few broken particles were observed in the 'as received' particulate composites. Although orientation of high aspect ratio particles was observed, the majority of the particles had aspect ratios approaching unity; thus orientation of the particles along the rolling direction was not an issue. Bands of high volume percent SiC_p and intermetallics, also observed in the whisker material, were evident. The grain size in the whisker material was smaller than that in the particulate material, i.e., 1.5 and 2.5 μm, respectively. Transmission electron microscopy revealed faulting and voids in both the whisker and particulate reinforcement phase, but the SiC/Al interface appears un-contaminated. Precipitation was rarely observed at the SiC/Al interface in either whisker or particulate materials [25].

Fatigue crack propagation tests were performed using C(T) specimens along the guidelines of ASTM Standard E647-86a, [26] for crack growth rates from 10^{-12} to 10^{-4} m per cycle. Tests were carried out controlled room air (22°C, relative humidity, 45%) at a sinusoidal frequency of 50 Hz. Crack lengths were

measured using the electrical potential difference method as described in the standard; a back-face strain gage was employed to record specimen compliance [27]. The compliance data were acquired using back-face strain readings averaged in situ over four cycles for the full range of crack growth rates. The closure load was determined manually from the compliance data with the closure load defined as the load at which the compliance curve deviated significantly from linearity under decreasing load. The stress intensity factor at closure, K_{cl}, was calculated from the crack length and the closure load following ASTM E-399 [24]. Tests were performed at two different stress ratios, $R = 0.7$ and 0.1 where R is the ratio of the minimum to maximum stress intensity factor in each cycle, $R = K_{min}/K_{max}$, for each aging condition in both the L-T and T-L orientations [24]. Initial tests of the 15% SiC_w/Al in the L-T orientation resulted in large scale crack deflection similar to that observed by Lee [20] and Ratnaparkhi and Rack, [21] rendering the tests un-interpretable. The introduction of side grooves on the specimen and careful alignment of the load train, however, produced an acceptable straight crack path.

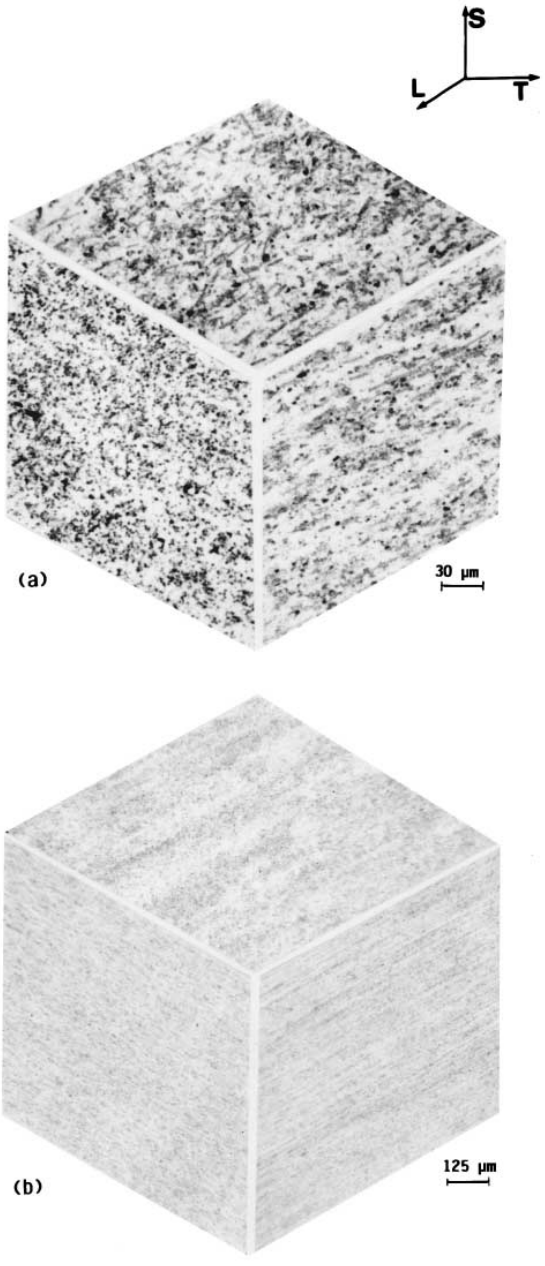

Fig. 1. Reinforcement distribution for 15% SiC_w/2124, as received; (a) larger whisker can be seen to be aligned along the L direction, (b) layered regions of high volume percent resulting from manufacture can be seen at lower magnification.

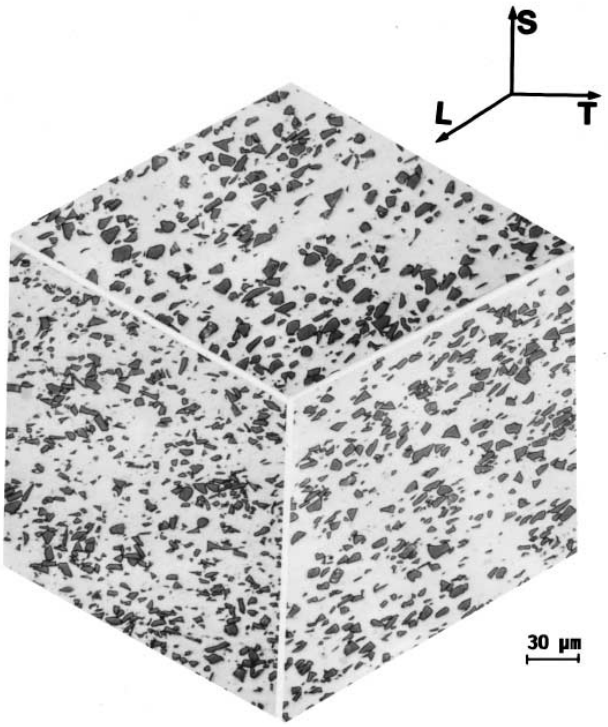

Fig. 2. 20% SiC_p/2124 aluminum composite, particulate structure and distribution within the matrix, as received.

Thresholds were approached using an automated load shedding procedure with the K gradient adjusted by the relationship [28],

$$\Delta K = \Delta K_0 \, e^{C(a - a_0)}, \quad (1)$$

where $\Delta K = K_{max} - K_{min}$ is the nominal stress intensity range, a is the instantaneous crack length, a_0 is the initial crack length, ΔK_0 is the initial stress intensity range and C is a constant, $C = -0.12$. Verification of the obtained curves was established by increasing ΔK from threshold with $C = 0.15$ after load shedding; both increasing and decreasing curves were found to be coincident. Crack growth rates are presented in terms of the nominal stress intensity range which was puted for the C(T) specimen as per ASTM E-399 [24].

Fatigue crack path profiles were examined by sectioning the specimen at the midpoint of the thickness. Cracks were infiltrated with epoxy, polished and examined in the JEOL JSM-35CF scanning electron microscope. Low accelerating voltages of about 5 kV (using a LaB_6 filament) produced excellent contrast between the reinforcement and the matrix. Crack lineal roughness—defined as the total length of the crack path divided by the projected length in the growth direction—was measured on selected specimens for each regime of crack propagation rates. The percentages of broken reinforcement and growth near the reinforcement/matrix interface were also determined. Fatigue crack fracture surfaces were examined using an ISI WB-6 scanning electron microscope, and the projected area percent of SiC was measured on these surfaces [29].

3. Experimental results

The dependence of fatigue crack propagation rates (FCPR) upon the applied stress intensity range, ΔK, is illustrated in Figs. 3–7 for all testing conditions. Crack closure information in the form of the ratio of the stress intensity at closure to the maximum stress intensity, K_{cl}/K_{max} vs. ΔK, is shown in each case for $R = 0.1$. Closure was not observed in the compliance data for tests performed at $R = 0.7$. Closure ratio data for all the materials exhibit the same general form, reflecting a K_{cl} that is constant with increasing ΔK. In the figures a linear fit (with slope held to -1) of the closure data is shown with the average K_{cl} for the material calculated from the intercept. Separate plots of K_{cl} versus ΔK show that K_{cl} is indeed nearly constant for the range of ΔK shown [30].

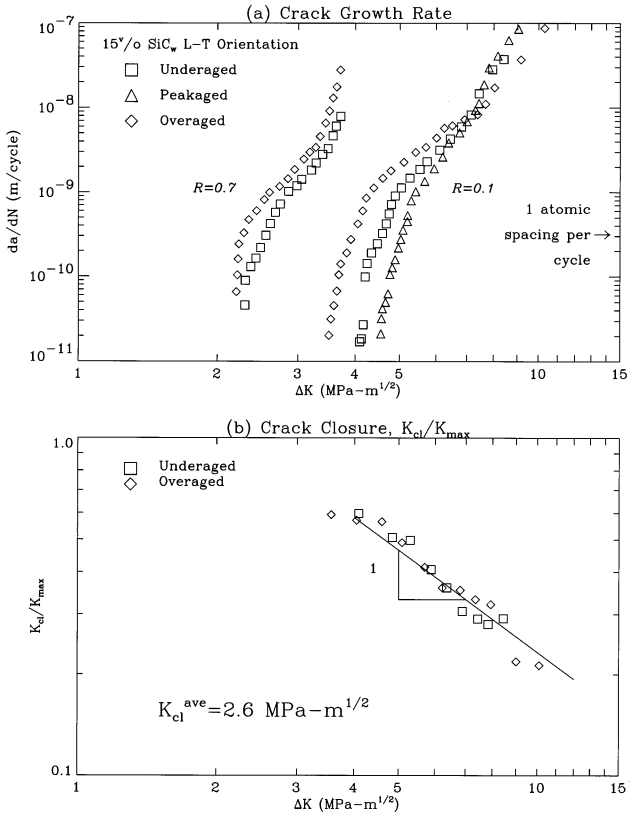

Fig. 3. Fatigue response of 15% SiC_w/2124 in the L-T orientation including (a) fatigue crack propagation rates for $R = 0.1$ and 0.7 and (b) closure ratio data for $R = 0.1$.

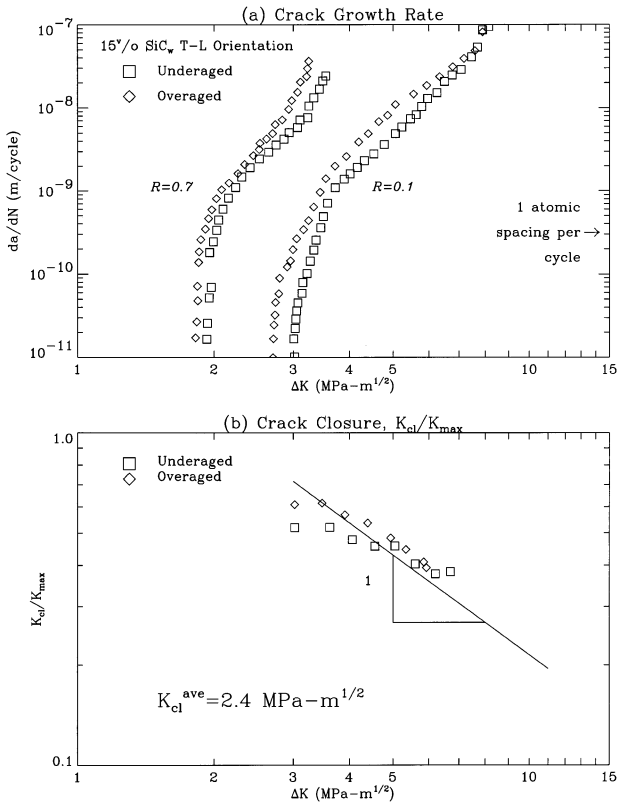

Fig. 4. Fatigue response of 15% SiC_w/2124 in the T-L orientation including (a) fatigue crack propagation rates for $R = 0.1$ and 0.7 and (b) closure ratio data for $R = 0.1$.

In the Paris Law regime, i.e., typically between 10^{-9} and 10^{-6} m per cycle, the composites exhibit behavior similar to the unreinforced wrought alloy [31] as shown in Fig. 8, but the lower fracture toughness of the composites restricts the linear portion of the curve. Consequently, crack growth resistance in the composite is inferior to that in the unreinforced metallic alloy at high ΔK as the crack growth instability is reached at lower K_{max} values due to the reduced toughness. Conversely, at low crack growth rates the composites exhibit superior performance; specifically, fatigue thresholds are higher in the composites than in the unreinforced P/M alloy, as shown in Fig. 8. However, crack behavior in the composites is only nominally higher than in the wrought alloy (Fig. 8). A

summary of threshold, ΔK_{th}, measurements is presented in Table 3. As can be seen in Figs. 3–8, thresholds are reduced with decreasing volume percent of reinforcement at $R = 0.1$ whereas they are essentially constant at $R = 0.7$ at $\Delta K_{th} \approx 2$ MPa-m$^{1/2}$. The 15% whisker material exhibits a threshold equivalent to the threshold of the 20% particulate composite at $R = 0.1$, while the 30% material exhibits a higher threshold than both 15 and 20% materials at that load ratio (Fig. 8). Anisotropy is less pronounced in the particulate reinforced composites, compared to the whisker reinforced alloys. For the 30% SiC_p material it can been seen that whereas the different orientations are indistinguishable at $R = 0.7$, at $R = 0.1$ the threshold values for the T-L orientations are slightly lower than the L-T orientations at comparable aging treatments (Fig. 9). For the 15% SiC_w, a much larger variation can be seen between the L-T and T-L orientations (Fig. 10). At both $R = 0.1$ and 0.7, the T-L orientation shows a significantly lower ΔK_{th} for this material.

Comparisons to the data of Shang and Ritchie [10,11] and Botstein et al. [19] indicate several interesting results. In Fig. 11 the growth rate data for the 20% SiC_p material studied here is compared with the 20% SiC_p material of Shang and Ritchie. The peak-aged material in this study has a nominal reinforcement

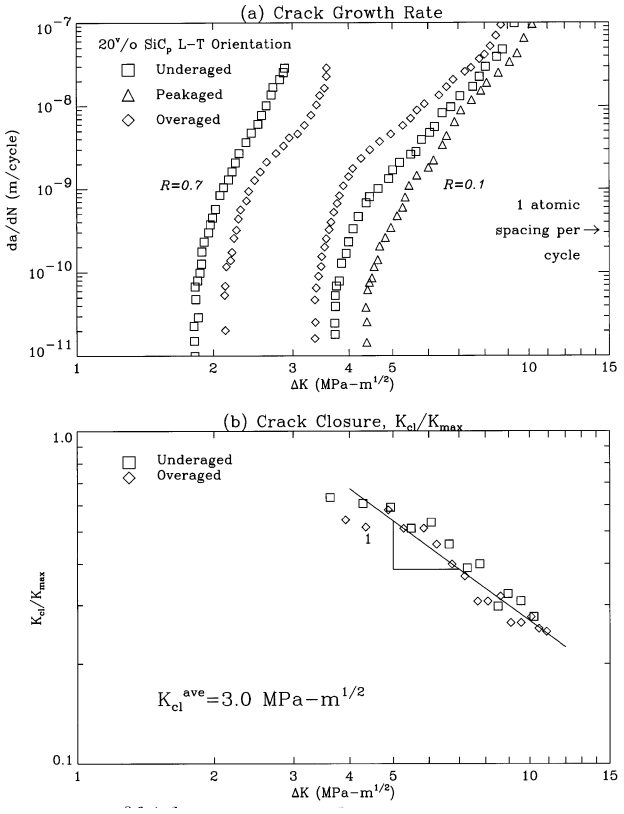

Fig. 5. Fatigue response of 20% SiC_p/2124 in the L-T orientation including (a) fatigue crack propagation rates for $R = 0.1$ and 0.7 and (b) closure ratio data for $R = 0.1$.

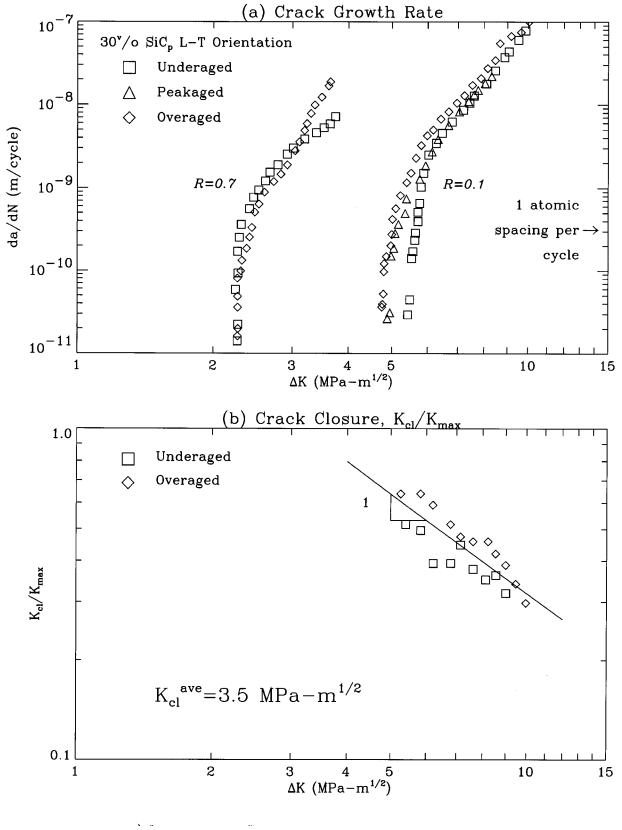

Fig. 6. Fatigue response of 30% SiC_p/2124 in the L-T orientation including (a) fatigue crack propagation rates for $R = 0.1$ and 0.7 and (b) closure ratio data for $R = 0.1$.

diameter of 10 μm while the peak-aged coarse and fine materials of Shang and Ritchie are ~16 and ~5 μm in diameter, respectively. It is seen in the figure that the material behavior in this study resembles that of the larger diameter reinforcement material of Shang and Ritchie. Although data for the closure loads were not available for the peak-aged condition, a comparison of K_{cl} is made between the data of Shang and Ritchie and that for the over-aged and under-aged conditions from this study. In Fig. 11(b), it can be seen that the closure behavior for the coarse material of Shang and Ritchie is similar to that of the present alloys. The solid line indicates the expected results for a constant $K_{cl} = 3.0$ MPa-m$^{1/2}$. The smaller reinforcement displays much lower closure loads and a different trend altogether. In Fig. 12, the results of Botstein et al. for an Al 2014-40% SiC_p material are presented with the growth rate data gathered here for a 30% SiC_p material; closure data from Botstein et al. were not reported. It is seen that the threshold value is much higher, $\Delta K_{th} \approx 7$ MPa-m$^{1/2}$, in the 40% material and the growth rates are slightly higher in the Paris regime.

The enhanced threshold is in agreement with the trend in these results; a larger volume percent leads to a higher threshold, as shown in Table 3. The higher

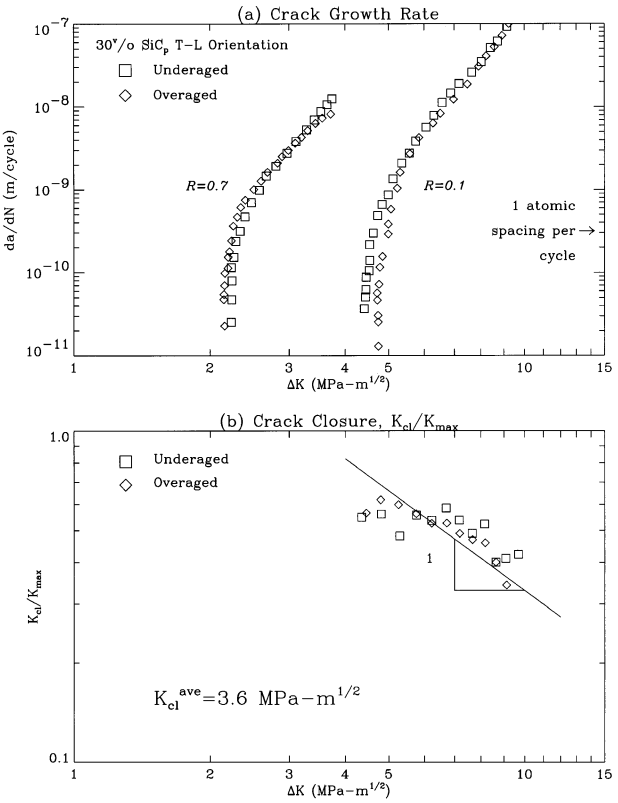

Fig. 7. Fatigue response of 30% SiC_p/2124 in the T-L orientation including (a) fatigue crack propagation rates for $R = 0.1$ and 0.7 and (b) closure ratio data for $R = 0.1$.

crack growth rate in the Paris regime is considered to be a reflection of the strong tendency toward particle clustering in the 40% material. Botstein et al. report striation markings in the clusters that may indicate faster crack growth there.

A typical crack profile in the particulate material is shown in Fig. 13. The percentage of crack growth near the SiC/Al interface is approximately equal to the reinforcement volume percent of the composite; however, it is apparent that the crack seeks out clusters of reinforcement and the corners of the more angular particles. Very few broken particles were observed; cracked particle percentages on the crack profile were measured at 2 and 5% for the 20 and 30 vol.% SiC_p composites, respectively. Lineal roughness measurements on the fatigue fracture surfaces were the same for both the 20 and 30% particulate composites. Values of 1.15 were measured in the threshold regime increasing with ΔK to values of 1.4 in the regime of crack growth close to instability. Quantitative investigation of the fatigue failure surfaces of the particulate composites resulted in projected SiC_p areal percentages. Values measured were approximately 6 and 10% for the 20 and 30 vol.% SiC_p materials, respectively, in all regimes of crack propagation. Auger spectroscopy of the exposed particles on the fatigue surfaces revealed no evidence of aluminum; the majority of such SiC particles failed by cleavage. There was evidence in the crack profiles that crack growth near the particle/matrix interface occurs in the matrix and not at the interface (Fig. 13); in fact, interface failure in the wake of the crack was rarely observed.

A typical whisker material crack profile is displayed in Fig. 14. As seen in the particulate reinforced materials, the crack is attracted to stress concentrators such as the whisker corners and high volume percent regions; indeed, cracks tended to deflect over relatively long distances in order to intersect clusters of whiskers. Fatigue surfaces revealed evidence of a small amount of whisker pull-out in the form of holes (Fig. 15) and protruding whiskers; however, pull-out lengths were small due to the short average length of the whiskers and the fact that the crack generally intersects whiskers near the tip. Aluminum was detected on the whiskers after pull-out, indicating that failure during pull-out did occur in the matrix.

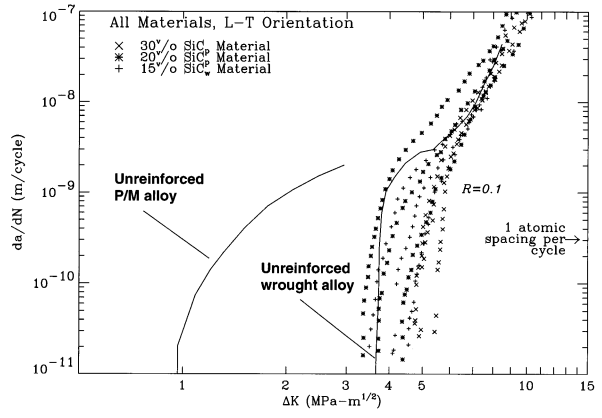

Fig. 8. Comparison of the fatigue crack growth rate for all of the materials tested in the L-T orientation with $R = 0.1$ to unreinforced P/M alloy [22] and the wrought alloy [31].

4. Discussion

As fatigue crack growth rates are clearly faster in the composites than in the unreinforced alloy at high ΔK levels because of their lower fracture toughness, the emphasis of the discussion here is directed toward near threshold behavior where closure mechanisms are dominant.

The fractographic evidence in Figs. 10–13 indicates that the SiC/Al interface in the aluminum matrix composites materials is strong enough to inhibit interfacial cracking and extensive pull-out of the whiskers; moreover, transmission electron microscopy revealed no evidence of precipitation on the interface or any other degradation of the interface during the thermomechanical treatment of the composites. This fact combined

Table 3
Threshold data for SiC/Al 2124 composites

Vol. %	Orientation	Aging condition	ΔK_{th} Threshold (MPa$\sqrt{m}$)		
			$R = 0.1$	$R = 0.1$, ΔK_{th}^{eff}	$R = 0.7$
O (wrought)	L-T	OA	2.0	—	—
		PA	2.4	—	—
		UA[a]	3.6	—	—
O (P/M)	L-T	OA	1.2	—	—
		PA	—	—	—
		UA[a]	1.0	—	1.0
15 SiC_w	L-T	OA	3.6	2.0	2.2
		PA	4.7	—	—-
		UA	4.2	1.8	2.3
	T-L	OA	2.7	1.3	1.8
		UA[a]	3.1	1.6	1.9
20 SiC_p	L-T	OA	3.4	2.1	2.2
		PA	4.5	—	—
		UA[a]	3.8	1.5	1.8
30 SiC_p	L-T	OA	4.9	2.1	2.3
		PA	5.1	—	—
		UA[a]	5.7	2.2	2.3
	T-L	OA	4.9	2.2	2.2
		UA	4.5	2.9	2.3

[a] T351 (other UA are T851).

with a lack of significant particle breakage ahead of the crack tip is a critically important factor in determining the fatigue crack growth resistance of these materials. Because the interface is strong and particle breakage is a minimum, the fatigue crack tends to grow around the ceramic reinforcement phase. Furthermore, the reinforcement morphology and distribution within the matrix add to the deflection of the crack by supplying stress concentrators, such as particle/whisker corners and reinforcement clusters, that attract crack growth. This results in a tortuous crack path. In addition, in the whisker reinforced materials evidence of minimal whisker pull-out can be seen (Fig. 14 and Fig. 15). Consequently, crack growth can be considered to be impeded in these composite materials by several mechanisms of crack tip shielding; namely crack closure due to the contact of surface asperities (roughness induced closure), crack deflection [32] and crack bridging due to limited whisker pull-out.

Roughness induced crack closure arises from the wedging action of fracture surface asperities. This mechanism is important when crack tip opening dis-

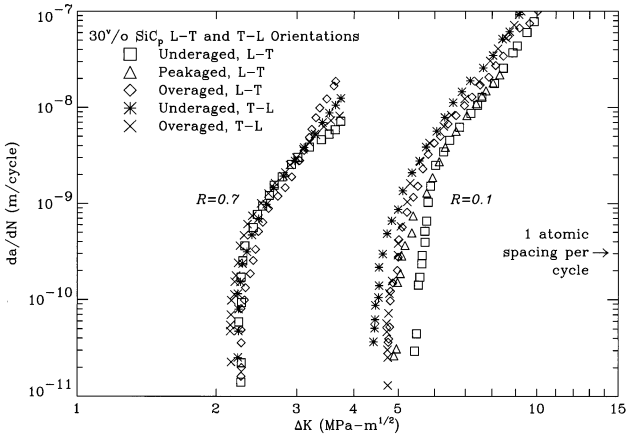

Fig. 9. Comparison of the fatigue crack growth rate for 30% SiC_p material when tested in the L-T and T-L orientations.

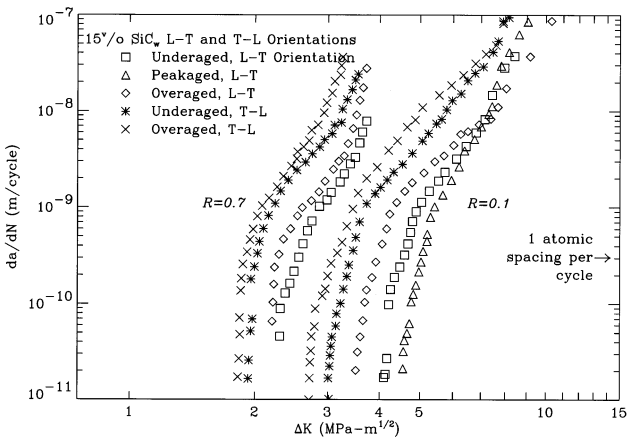

Fig. 10. Comparison of the fatigue crack growth rate for SiC_w material when tested in the L-T and T-L orientations.

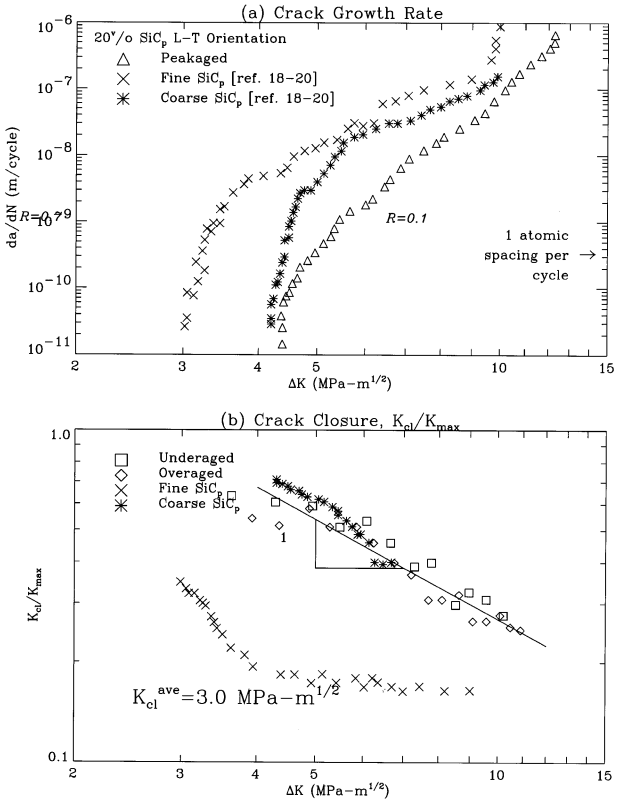

Fig. 11. Comparison of the fatigue crack growth rate for 20% SiC_p material with the data of Shang and Ritchie, [10,11] shown as 'Fine SiC_p' and 'Coarse SiC_p'.

placements, CTODs, are small and where significant crack tip shear displacements occur [33]. The resulting wedging action of fracture surface asperities is promoted by the crack path tortuousity from frequent crack deflection. The degree of tortuousity can be characterized by the lineal roughness and average crack deflection angle. Lineal roughness gives the ratio of the actual crack path length to the length projected along

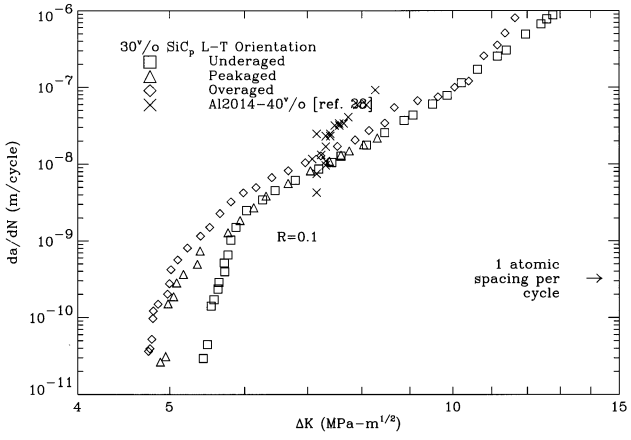

Fig. 12. Comparison of the fatigue crack growth rate for the 30% SiC_p material with the data of Botstein al. [19] shown as 'AL 2014-40°/o'.

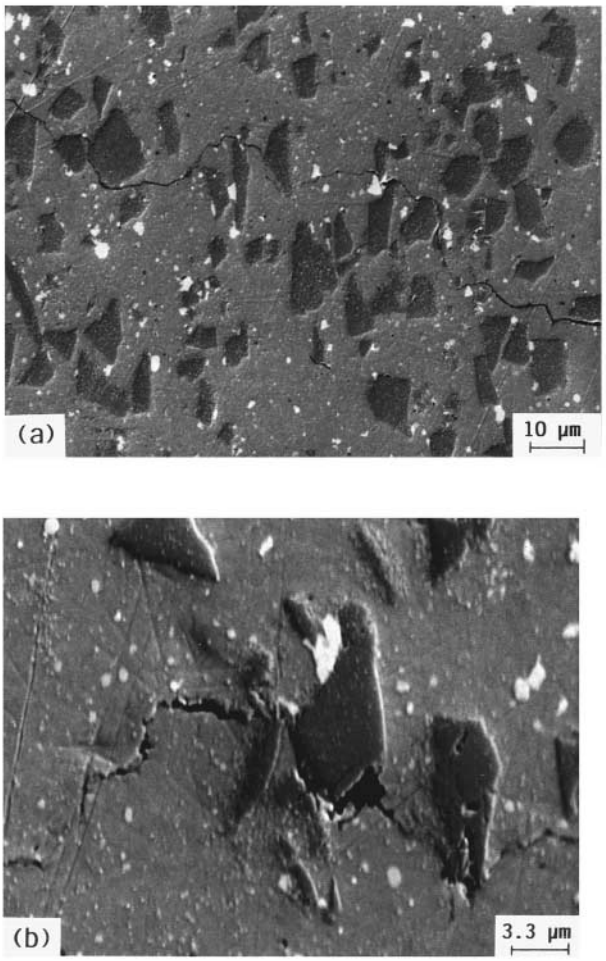

Fig. 13. (a) Exemplary crack profile in particulate reinforced aluminum 2124. (b) High magnification reveals aluminum left on the surface of particle after near interface crack growth. Crack growth is from left to right and the growth rate is approximately 5×10^{-9} m per cycle.

the macroscopic crack growth direction; it is not unrelated to the average deflection angle, but a more complete description is given by the two indicators taken together. Roughness induced closure is most effective at low stress intensity ranges, when CTODs are comparable with surface asperity sizes, at low load ratios (small CTOD), and when crack deflection mechanisms are active.

Since CTODs are minimized at near threshold levels, the load ratio dependence in this regime can generally be attributed to variations in crack closure, in the present composites primarily arising from roughness induced closure. With a lineal roughness of 1.15 and average deflection angle of 35–40°, the resulting surface asperities come into contact at a closure stress intensity factor, K_{cl}, greater than the minimum stress intensity factor, K_{min}, thereby reducing the effective, near-tip stress intensity range from $K_{max} - K_{min}$ to $K_{max} - K_{cl}$. In

fact, subtraction of closure effects in the crack tip driving force resulted in the normalization of differing R ratio data for all the cases reported here [30]; specifically, the dependence of fatigue crack growth rates upon effective stress intensity factor, $\Delta K^{\text{eff}} = K_{\max} - K_{\text{cl}}$, is very similar for $R = 0.1$ and $R = 0.7$. In Fig. 16 and Fig. 17 the crack growth rate data for the 30% SiCp and 15% SiCW materials tested is shown as function of ΔK^{eff} for both R ratios and orientations. Threshold values, $\Delta K^{\text{eff}}_{\text{th}}$, calculated in terms of ΔK^{eff} from the $R = 0.1$ data, coincided with those measured when $R = 0.7$ for all cases (Table 3), indicating that load ratio dependence is a largely associated with crack closure in these materials.

Crack deflection and meandering can act to impede crack growth in addition to roughness induced closure. At large CTODs, compared to the surface asperities for example, high lineal roughness and high crack deflection angles result in a reduction in the crack tip driving force by deviations of the crack path from the surface of maximum tensile stress. To assess the influence of crack deflection, Cotterell and Rice [34] have determined the local mode-I, k_1, and mode-II, k_2, stress intensity factors for a kinked (in-plane) mode-I crack growing under a nominal far-field stress intensity factor, K_{I}, at an angle of deflection θ to be

$$k_1 \approx \cos^3\left(\frac{\theta}{2}\right) K_{\text{I}} \quad \wedge \quad k_2 \approx \sin\left(\frac{\theta}{2}\right) \cos^2\left(\frac{\theta}{2}\right) K_{\text{I}}. \qquad (2)$$

Using the observed average angle of deflection in these materials, 35–40°, and calculating the effective crack tip stress intensity, k, using the maximum strain energy release rate criterion,

$$k = \sqrt{k_1^2 + k_2^2}$$

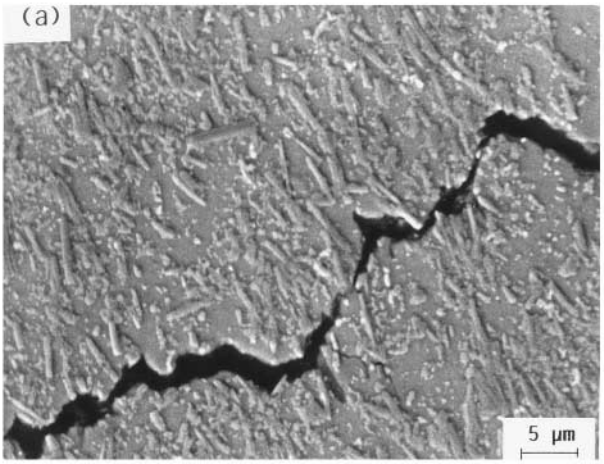

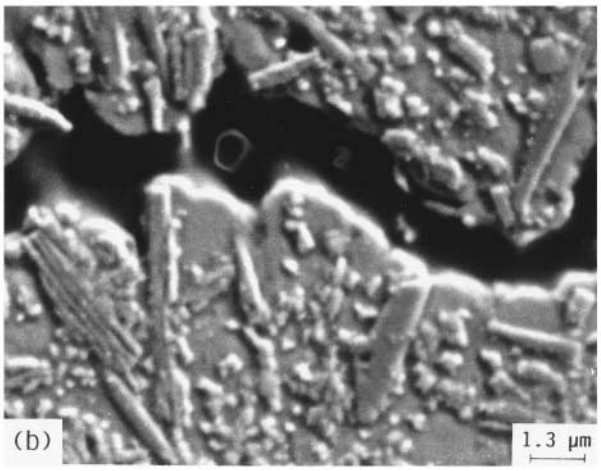

Fig. 14. (a) Exemplary whisker reinforced 2124 crack profile showing evidence of roughness induced closure. (b) High magnification reveals crack attraction toward whisker ends. Evidence of pull-out is observed. (Crack growth is from left to right and the growth rate is approximately 5×10^{-9} m per cycle).

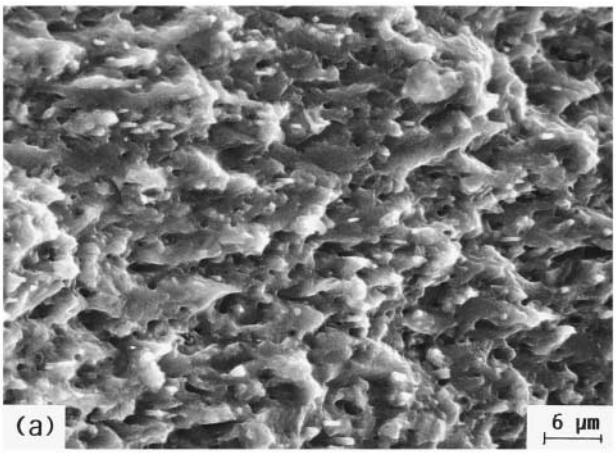

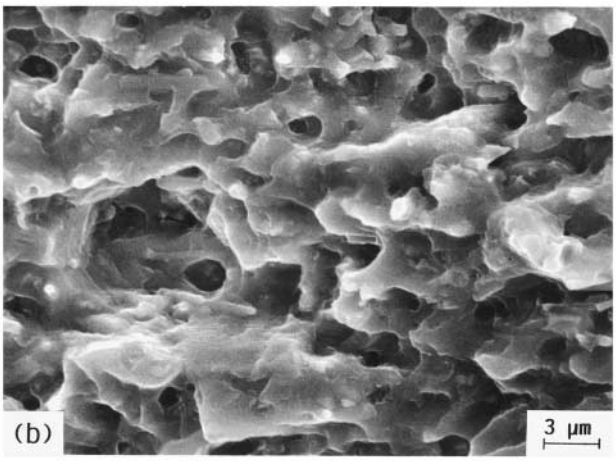

Fig. 15. Fatigue surface of 15% SiC_w/2124 in L-T orientation. Whisker ends and pull-out voids are evident. Crack growth is from left to right and the growth rate is approximately 5×10^{-9} m per cycle).

gives a ratio of effective crack tip stress intensity to nominal stress intensity of $k/K_I = 0.90$, a 10% reduction in driving force, which is negligible when compared to experimental scatter. However, somewhat larger effects may be expected for out-of-plane (i.e., twisting) deflection of the crack [32].

It should be noted that accounting for closure effects resulted in effective threshold values close to 2.0 MPa$\sqrt{m}$ for both the 20 and 30 vol.% SiC_p materials when $R = 0.1$ (the same value found when $R = 0.7$). Crack profiles showed no observable difference in the crack path near threshold for the two materials; in fact, lineal roughness measurements were equal. Calculation of the crack tip opening displacement at the closure stress intensity,

$$\mathrm{CTOD}_{cl} = \frac{4}{\pi}\frac{K_{cl}^2}{E\sigma_y}, \tag{3}$$

in both materials yielded relatively similar values of ~ 0.25 μm which is on the order of the average surface asperity height. Setting the CTOD_{cl} equal for both materials gives the ratio of the closure stress intensity factors,

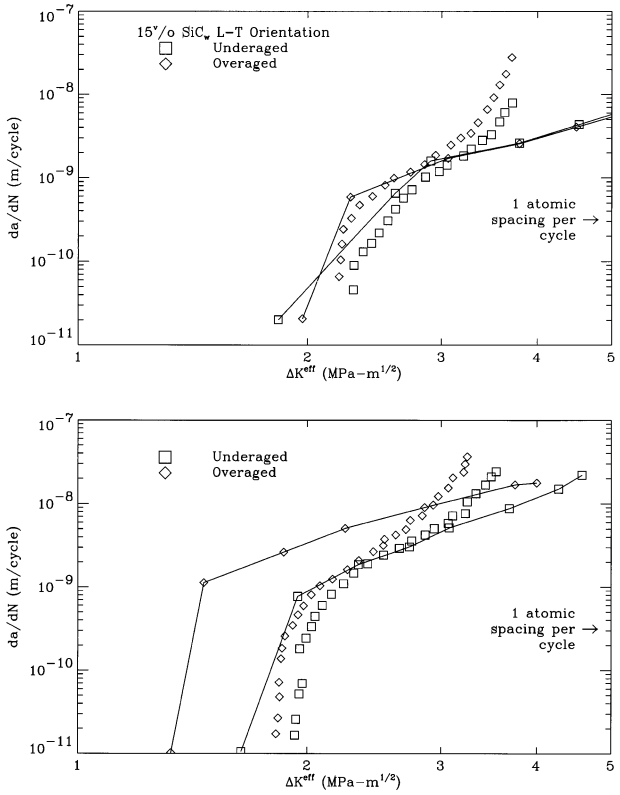

Fig. 16. Comparison of the fatigue crack growth rate for the 15% SiC_w material using ΔK_{th}^{eff}. Connected symbols represent the data taken when $R = 0.1$ and modified by the subtraction of closure effects; the other data is for $R = 0.7$.

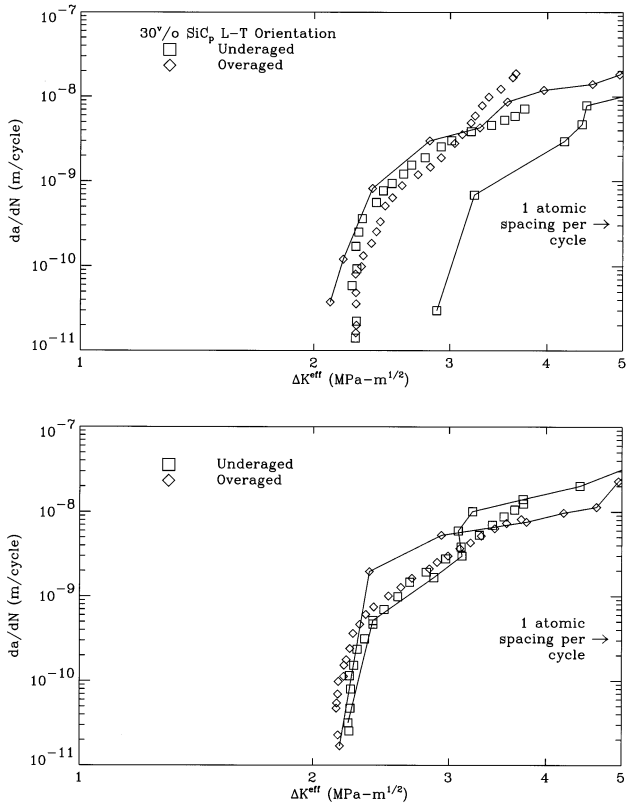

Fig. 17. Comparison of the fatigue crack growth rate for the 30% SiC_p material using ΔK_{th}^{eff}. Connected symbols represent the data taken when $R = 0.1$ and modified by the subtraction of closure effects; the other data is for $R = 0.7$.

$$\frac{K_{cl}^{(30\%)}}{K_{cl}^{(20\%)}} = \sqrt{\frac{E^{(30\%)}\sigma_y^{(30\%)}}{E^{(20\%)}\sigma_y^{(20\%)}}} \approx 1.2 \tag{4}$$

The observed ratio is 1.25. Thus, an increase in ΔK_{th} with the volume fraction of particulate is to be expected if the average asperity height on the fracture surface is the same in each material or if the roughness is the same in each case (as they are); the higher closure levels in the 30% SiC_p material, which result in higher ΔK_{th} values, are probably the result of the higher modulus.

Measurement of fatigue crack growth rates in the T-L orientation revealed no evidence of appreciable orientation effects in 30% SiC_p composite at both $R =$ 0.1 and 0.7. This lack of orientational dependence is considered to be a reflection of the relative mechanical isotropy of the particulate reinforced material and the relative geometric isotropy of the reinforcement.

In contrast to the particulate material, the 15% whisker material exhibited a marked orientation dependence in fatigue properties. Indeed, 25% lower threshold values were measured in the T-L orientation (compared to the L-T orientation) at $R = 0.1$. This effect can again be rationalized by variations in closure levels since at $R = 0.7$ no closure was observed), there was no orientational dependence of the measured threshold values.

Crack profiles for these conditions showed lower lineal roughness measurements for the T-L specimens due to the orientation of the whiskers along the crack growth direction. The CTOD at closure for the T-L orientation was approximately half that for the L-T orientation indicating that surface contact occurred at much smaller crack face separations. Therefore, the orientational dependence of ΔK_{th} in 15% SiC_w/Al is considered to be a result of the lower crack path roughness in specimens tested in the T-L orientation.

Finally, the 15% whisker material exhibits threshold values that are nominally the same as the 20% particulate material. This would suggest that more resistance to crack growth can be obtained in the L-T orientation by using whisker reinforcement instead of particulate. (The gains, however, are offset by the tendency for cracks to deflect and grow in the T-L orientation.) The reason for this difference in behavior is assumed to be related to a slightly higher crack path roughness in the 15% SiC_w, material and the added crack tip shielding effects of minimal bridging by pulled out whiskers.

5. Conclusions

1. The introduction of SiC particles or whiskers into aluminum 2124 P/M alloys results in an increase in the long crack threshold stress intensity ranges, ΔK_{th}, at both high and low R ratios, $R = 0.1$ and 0.7. However, at high ΔK levels the lower fracture toughness of the composites results in crack growth resistance inferior to that in the unreinforced alloys as K_{max} approaches K_{Ic}.
2. The apparent high strength of the SiC_p or SiC_w/aluminum 2124 interface resists failure causing fatigue cracks to propagate around the SiC reinforcement phase resulting in extensive crack deflection. Fatigue cracks appear to by-pass particles/whiskers in their path by growing in the matrix, near the interface. Consequently, the crack path is more tortuous in the composites than in the unreinforced matrix.
3. The particle morphology and distribution within the matrix plays an important role in the mechanisms of fatigue crack growth in the composites. Fatigue cracks are to attracted to stress concentrators such as whisker ends, particle corners and reinforcement clusters resulting in deflection of the crack and a consequently tortuous crack path.
4. The particle strength is apparently sufficient to minimize particle breakage in the crack path. High particle strength prevents particle breakage which leads to crack deflection around the reinforcement. As a result, in contrast to reports on other Al/SiC_p, [11] particle breakage is not a significant factor in determining the fatigue crack growth resistance of the present composites.
5. Variation of ΔK_{th} with volume percent in the particulate reinforced materials at $R = 0.1$ is attributed to differences in K_{cl}. Closure levels appear to be determined by a roughness mechanism and a $CTODC_{cl}$, that is independent of volume percent. Roughness is dependent upon the size, morphology and distribution of the reinforcement.
6. When $R = 0.1$, ΔK_{th} values measured in the whisker materials for crack propagation in the L-T orientation, i.e., perpendicular to the reinforcement alignment direction, are higher than those measured in the T-L orientation, i.e., along the reinforcement alignment direction. This effect is explained in terms of lower crack path roughness. In the particulate material no appreciable orientation effects are observed.
7. Whisker materials exhibit higher thresholds when measured along the rolling direction (the L-T orientation) compared to particulate materials. This effect is attributed to crack tip shielding by whisker pull-out and roughness induced closure.
8. A dependence on orientation, reinforcement morphology and volume percent of ΔK_{th} at $R = 0.7$ is not observed in the SiC_p or SiC_w, composites due to the ineffectiveness of closure mechanisms and a minimal effect of crack deflection.

Acknowledgements

This work was supported by the Director, Office of Energy Research, Office of Basic Energy Services, Materials Sciences Division, the US Department of Energy, under Contract No. DE-AC03-76SF00098.

References

[1] J. Lee, I.B. Cutler, Ceramic Bull. 54 (1975) 195.
[2] D.M. Knowles, T.J. Downes, J.E. King, Acta Metall. Mater. 41 (4) (1993) 1189.
[3] V.K. Karma, S.V. Kamat, M.K. Jain, V.V. Bhanu Prasad, Y.R. Mahajan, J. Mat. Sci. 28 (1993) 477.
[4] Y. Sugimura, S. Suresh, Met. Trans. A 23A (1992) 2231.
[5] D.M. Knowles, J.E. King, Mat. Sci. Tech. 8 (1992) 500.
[6] D.L. Davidson, Met. Trans. A 22A (1991) 97.
[7] M. Levin, B. Karlsson, Mat. Sci. Tech. 7 (1991) 596.
[8] D.M. Knowles, J.E. King, Acta Metall. Mater. 39 (5) (1991) 793.
[9] J.K. Shang, R.O. Ritchie, Acta Metall. 37 (8) (1989) 2267.
[10] J.K. Shang, R.O. Ritchie, Metall. Trans. A 20A (1989) 897.
[11] J.K. Shang, W. Yu, R.O. Ritchie, Mater. Sci. Eng. A 102 (1988) 181.
[12] W.A. Logsdon, P.K. Liaw, Eng. Fract. Mech. 24 (1986) 737.
[13] D.L. Davidson, Metall. Trans. A 18A (1985) 1105.
[14] C.R. Crowe, D.F. Hasson, in: R.C. Gifkins (Ed.), Proc. 6th Int. Conf. on the Strength of Metals and Alloys, Vol. 2, Melbourne, August 16–20, 1982, Pergamon, Oxford, 1982, p. 859.
[15] D.F. Hasson, C.R. Crowe, in: W. Harrigan, J. Strife, A.K. (Eds.), Proc. 5th Int. Conf. on Composite Materials, Metallurgical Society of AIME, Warrendale, PA, 1985, p. 147.

[16] D.R. Williams, M.E. Fine, in: W. Harrigan, J. Strife and A.K. Dhingra (Eds.), Proc. 5th Int. Conf. on Composite Materials, Metallurgical Society of AIME, Warrendale, PA, 1985, p. 639.
[17] S.S. Yau, G. Mayer, Mater. Sci. Eng. 82 (1986) 45.
[18] T.E. Steelman, A.D. Bakalyar, L. Konopka, Tech. Rep. AFWAL-TR-86, 1986, Rockwell International Corporation, Los Angeles, CA.
[19] O. Botstein, R. Arone, B. Shpigler, Mater. Sci. Eng. A128 (1990) 15.
[20] E.U. Lee, Metall. Trans. A 21A (1990) 1783.
[21] P.L. Ratnaparkhi, H.J. Rack, Mater. Sci. Eng. A A129 (1990) 11.
[22] T. Christman, S. Suresh, Acta Met. 36 (1988) 1691.
[23] T.G. Nieh, R.F. Karlak, Scripta Met. 18 (1984) 25.
[24] ASTM Stand, E399-83, Vol. 3.01, 1987, p. 680.
[25] L.H. Edelson, Ph.D. Thesis, University of California, Berkeley, CA, 1989.
[26] ASTM Stand, E 647-86A, Vol. 3.01, 1987, p. 899.
[27] W.F. Deans, C.E. Richards, J. Test Eval. 7 (1979) 147.
[28] A. Saxena, S.J. Hudak Jr, J.K. Donald, D.W. Schmidt, J. Test Eval. 6 (1978) 167.
[29] J.R. Pickens, J. Gurland, in: E.E. Underwood, R. deWitt, G.A. Moore (Eds.), Proc. Fourth International Conference on Stereology, NBS 431, National Bureau of Standards, 1976, p. 269.
[30] J.J. Mason, M.S. Thesis, University of California, Berkeley, 1988.
[31] R.O. Ritchie, W. Yu, D.K. Holm, A.F. Blom, in: J.C. Newman Jr., W. Elber (Eds.), Mechanics of Fatigue Crack Closure, ASTM STP 982, American Society for Testing and Materials, Philadelphia, 1988, p. 300.
[32] S. Suresh, Metall. Trans. A 14A (1983) 2375.
[33] R.O. Ritchie, Mater. Sci. Eng. A 103 (1988) 1034.
[34] B. J.R. Rice, Int. J. Fract. 16 (1980) 155.